Review

Magnetostructural D-correlations and their impact to single-molecule magnetism

Ján Titiš *, Cyril Rajnák, Roman Boča

Posted Date: 27 September 2023

doi: 10.20944/preprints202309.1797.v1

Keywords: Zero-field splitting, Magnetostructural correlations, Ni(II) complexes, Co(II) complexes, Single-molecule magnets

Review

Magnetostructural D-Correlations and Their Impact to Single-Molecule Magnetism

Ján Titiš [1,*], Cyril Rajnák [1] and Roman Boča [2]

[1] Department of Chemistry, FPV, University of SS Cyril and Methodius, 91701 Trnava, Slovakia
[2] Faculty of Health Sciences, University of SS Cyril and Methodius, 91701 Trnava, Slovakia
* Correspondence: jan.titis@ucm.sk

Abstract: Functional dependence of the axial zero-field splitting parameter D with respect to a properly chosen geometrical parameter (D_{str}) in metal complexes is termed the Magnetostructural D-Correlation. In mononuclear hexacoordinate Ni(II) complexes with the ground electronic term $^3B_{1g}$ ($^3A_{2g}$ in the regular octahedron) it proceeds along two intercepting straight lines allowing to predict the sign and magnitude of the D-parameter by knowing the X-ray structure alone; D_{str} is constructed from the metal-ligand bond lengths. In hexacoordinate Co(II) complexes it is applicable only in the segment of the compressed bipyramid where the ground electronic term $^4B_{1g}$ is orbitally non-degenerate so that the spin Hamiltonian formalism holds true. The D *vs* D_{str} correlation is strongly non-linear and it is represented by a set of decreasing exponentials. In tetracoordinate Co(II) complexes, on the contrary, the angular distortion from the regular tetrahedron is crucial so that the appropriate structural parameter D_{str} is constructed of bond angles. All of these empirical correlations originate in the electronic structure of metal complexes that can be modelled by the generalized crystal-field theory. As the barrier to spin reversal in the single-molecule magnets is proportional to the D-value, for a rational tuning and/or prediction of the single-molecule magnetic behavior knowledge/prediction of the D-parameter is beneficial. In this review, we present the statistical processing of an extensive set of structural and magnetic data of Co(II) and Ni(II) complexes, which were published over the past 15 years. Magnetostructural D-correlations defined for this data set are reviewed in detail.

Keywords: zero-field splitting; magnetostructural correlations; Ni(II) complexes; Co(II) complexes; single-molecule magnets

1. Introduction

Though a dodecanuclear plaquette-type complex, $[Mn^{III}_8Mn^{IV}_4O_{12}(ac)_{16}(H_2O)_4]\cdot 2Hac\cdot 4H_2O$, abbr. Mn12ac, was synthesized in 1980, its unusual magnetic properties were reported in 1991 and later termed as new class of magnetic materials–single molecule magnets [1–4]. These systems show quantum effects of which the most important is a slow magnetic relaxation. Slow means that the extrapolated relaxation time (time extrapolated to infinity temperature) is typically of the order $\tau_0 \sim 10^{-6}$–10^{-8} s, unlike to spin glasses where $\tau_0 < 10^{-20}$ s [4,5]. At temperature low enough the system retains its magnetization for a time long enough to find potential applications in recording technique. In course of time, a plethora 3d-metal complexes were identified as single-molecule magnets; for instance systems of different nuclearity cover Mn2, Mn3, Mn4, Mn6, Mn7, Mn8, Mn9, Mn10, Mn12, Mn16, Mn18, Mn21, Mn22, Mn25, Mn26, Mn30, Mn84, Fe4, Fe8, Fe9, Fe10, Fe11, Fe19, Co4, Co6, Ni4, Ni8, Ni12, Ni21, MnCu, V4, MnMo6, Mn2Cr, Mn2Fe, Mn2Ni2, Ni3Cr, Mn4Re4, Cu6Fe8, Co9W6, Co9Mo6, Mn8Fe4, etc. [6]. It can be concluded that high nuclearity is not an ultimate demand for single-molecule magnetic behaviour since many mononuclear complexes of Cr(III), Mn(III), Mn(II), Fe(III), Fe(II), Fe(I), Co(II) and Ni(II) possessing the spin S = 1 through 5/2 also show slow magnetic relaxation [7–9]. Moreover, some S = 1/2 spin systems, such as V(IV), low-spin Mn(IV), low-spin Co(II), low-spin Ni(III), Ni(I) and Cu(II), exhibit the slow magnetic relaxation as well [10–13]. Slow magnetic relaxation and single-molecule magnetism was identified among 4f-complexes (mononuclear and polynuclear) as well as heterometallic 4f-3d complexes; for instance, Tb1, Dy1,

Preprints (www.preprints.org) | NOT PEER-REVIEWED | Posted: 27 September 2023 doi:10.20944/preprints202309.1797.v1

TbCu, Dy2, Dy4, Dy6Mn6, Dy4Mn11, and many others were classified as single-molecule magnets [6].

Unlike to classical magnetic materials (like ferrites widely used in daily recording technique and many useful tools) the single-molecule magnet retains its magnetization due to the magnetic anisotropy. The magnetic anisotropy in single crystals is defined through the non-isotropic magnetization tensor having at least two main-axes components different, or the non-isotropic susceptibility tensor. In molecules, the spin-spin interaction tensor, when rotated to its main axes, possesses the diagonal elements

$$\hat{H}^{ss} = \hbar^{-2}(D_{xx}\hat{S}_x^2 + D_{yy}\hat{S}_y^2 + D_{zz}\hat{S}_z^2) \tag{1}$$

that define two eccentricity parameters:

(a) the axial zero-field splitting (ZFS) parameter D

$$D = (-D_{xx} - D_{yy} + 2D_{zz})/2 \rightarrow (3/2)D_{zz} \tag{2}$$

(b) the (ortho)rhombic ZFS parameter E

$$E = (D_{xx} - D_{yy})/2 \tag{3}$$

These two parameters modify (split) the ground-state energy levels in the absence of the magnetic field and they are responsible for the magnetic anisotropy. The magnetic anisotropy manifests itself in the way that with increasing magnetic field the magnetization components as well as the magnetic susceptibility (Cartesian) components develop differently.

Using the ZFS parameters, the spin-spin interaction can be rewritten to the form

$$\hat{H}^{ss} = \hbar^{-2}[D(\hat{S}_z^2 - \hat{S}^2/3) + E(\hat{S}_x^2 - \hat{S}_y^2)] \tag{4}$$

and usually a constraint $|D| \geq 3E \geq 0$ is maintained. For a uniaxial system (like D_{4h} or C_{4v}) the effective spin-Hamiltonian collapses to

$$\hat{H}^{aniso} = \hbar^{-2} D_S \hat{S}_z^2 \tag{5}$$

giving rise to the energy levels depending upon the magnetic quantum number M

$$\varepsilon = D_S M^2 \tag{6}$$

(In these formulae it is emphasized that we are working in the strong exchange limit for polynuclear systems, so that the D-parameter depends upon the (good) total molecular spin quantum number S, hence D_S). When $D_S > 0$ (easy-plane anisotropy) a model of a particle in the potential box is appropriate: a fast relaxation from the state $M = -S$ to $M = 0$ (or $M = \pm 1/2$) proceeds and the magnetic record disappears. On the contrary, when $D_S < 0$ (easy-axis anisotropy) a model of a particle in the double potential is applicable; the two minima are separated by a barrier to spin reversal $\Delta E = |D_S| S^2$ (or $\Delta E = |D_S| S^2 - |D_S|/4$ for the half-integral spin) and thermal activation mechanism of the relaxation, or tunnelling mechanism apply. For this reasoning a deep knowledge about the D_S-parameter is a key factor for a rational synthesis of single-molecule magnets with aimed properties. The rhombic ZFS parameter E_S is also in the play through the term $E_S(\hat{S}_x^2 - \hat{S}_y^2)$ and it causes a further modification of the energy levels and consequently the single-molecule magnetic behavior.

2. Spin-Hamiltonian Formalism

The spin-Hamiltonian (SH) formalism is applicable when the ground electronic term is orbitally non-degenerate (e.g., $^3A_{2g}$, $^4B_{1g}$). In this model the electronic wave function is substituted by spin-only kets $|S, M_S\rangle$. This very restricted basis set is under the action of operators covered by three leading terms: the spin Zeeman term, the orbital Zeeman term, and the spin-orbit interaction term

$$\hat{H}' = \hbar^{-1}\mu_B g_e(\vec{S}\cdot\vec{B}) + \hbar^{-1}\mu_B(\vec{L}\cdot\vec{B}) + \hbar^{-2}\lambda(\vec{L}\cdot\vec{S}) \tag{7}$$

Preprints (www.preprints.org) | NOT PEER-REVIEWED | Posted: 27 September 2023 doi:10.20944/preprints202309.1797.v1

Here g_e is the spin-only magnetogyric factor and $\lambda = \pm\xi / 2S$ is the spin-orbit splitting parameter within the ground electronic term dependent upon the spin-orbit coupling constant ξ (the minus sign applies for the configurations d^n more than half-full). Then the second-order perturbation theory yields the contribution [14]

$$\hat{H}^S = \hbar^{-2}(\vec{S}\cdot\bar{\bar{D}}\cdot\vec{S}) + \hbar^{-1}\mu_B(\vec{B}\cdot\bar{\bar{g}}\cdot\vec{S}) + (\vec{B}\cdot\bar{\bar{\kappa}}\cdot\vec{B}) \tag{8}$$

To this end, three magnetic tensors contribute:

- D–tensor (tensor of the spin-spin interaction)

$$D_{ab} = \lambda^2 \Lambda_{ab} \quad \text{[energy]} \tag{9}$$

- g–tensor (tensor of the magnetogyric ratio)

$$g_{ab} = g_e\delta_{ab} + 2\lambda\Lambda_{ab} \quad \text{[dimensionless]} \tag{10}$$

- κ–tensor (tensor of the temperature-independent paramagnetism)

$$\kappa_{ab} = \mu_B^2 \Lambda_{ab} \quad \text{[energy} \times \text{induction}^{-2}\text{]} \tag{11}$$

All of them are constituted of the Λ-tensor (tensor of the angular momentum unquenching)

$$\Lambda_{ab} = -\hbar^{-2} \sum_{K\neq 0} \frac{\left\langle 0\left|\hat{L}_a\right|K\right\rangle\left\langle K\left|\hat{L}_b\right|0\right\rangle}{E_K - E_0} \quad \text{[energy}^{-1}\text{]} \tag{12}$$

where the summation runs over all excited states (electronic terms). The scalar product of the vectors and tensors can be developed as follows

$$\hat{H}^S = \sum_a^{x,y,z}\sum_b^{x,y,z} \{\hbar^{-2}\lambda^2\Lambda_{ab}\hat{S}_a\hat{S}_b + \hbar^{-1}\mu_B B_a(g_e\delta_{ab} + 2\lambda\Lambda_{ab})\hat{S}_b + \mu_B^2\Lambda_{ab}B_aB_b\} \tag{13}$$

In the zero magnetic field we arrive at the formulae (1) through (4) that are widely used in analysing the magnetic data (susceptibility and magnetization) as well as the spectroscopic data such as Electron-Spin-Resonance (ESR) or Far-Infra-Red (Far-IR) spectra referring to electronic transitions.

For degenerate ground electronic terms of the T-type the above formalism is inappropriate and one is left to pass beyond the spin-Hamiltonian formalism. In early stages it was covered by Griffith and Figgis theory, respectively, dealing with the ground $T_{1(g)}$ or $T_{2(g)}$ terms, eventually under the symmetry lowering and configuration interaction [15,16]. A more complete approach that involves all members of the d^n-electron configuration has been outlined by König-Kremer theory [17]. This theory was reformulated and simplified elsewhere [18,19].

3. Electronic Structure of 3d-Complexes

Almost complete description of the energy levels in metal d- or f-complexes can be obtained by considering five operators acting to the basis set of free-atom terms $\left|l^n v L S M_L M_S\right\rangle$ with the seniority number v:

(a) the interelectron repulsion

$$H_{IJ}^{ee} = \left\langle l^n v L S M_L M_S \left| \hat{V}^{ee} \right| l^n v' L' S' M_L' M_S' \right\rangle = \delta_{M_L,M_L'}\delta_{M_S,M_S'}\delta_{L,L'}\delta_{S,S'}$$
$$\left\langle l^n v L S \left\| \sum_{i=1}^{n}\sum_{j>i}^{n}\sum_{k=0,2,4}^{2l} F_{ll}^k \sum_{q=-k}^{+k}(-1)^q \hat{C}_{-q}^k(i)\hat{C}_q^k(j) \right\| l^n v' L' S' \right\rangle \tag{14}$$

(b) the crystal-field potential

Preprints (www.preprints.org) | NOT PEER-REVIEWED | Posted: 27 September 2023 doi:10.20944/preprints202309.1797.v1

$$H_{IJ}^{\mathrm{cf}} = \left\langle l^n vLSM_L M_S \left| \hat{V}^{\mathrm{cf}} \right| l^n v'L'S'M'_L M'_S \right\rangle = \delta_{S,S'}\delta_{M_S,M'_S}$$
$$\left\langle l^n vLSM_L M_S \left| \sum_{i=1}^{n}\sum_{K=1}^{N} z_K \sum_{k=0,2,4}^{2l} F_k(R_K) \sum_{q=-k}^{+k} (-1)^q \hat{C}_{-q}^k(K)\hat{C}_q^k(i) \right| l^n v'L'S'M'_L M'_S \right\rangle \quad (15)$$

(c) the spin-orbit interaction

$$H_{IJ}^{\mathrm{so}} = \left\langle l^n vLSM_L M_S \left| \hat{V}^{\mathrm{so}} \right| l^n v'L'S'M'_L M'_S \right\rangle$$
$$= \left\langle l^n vLSM_L M_S \left| \hbar^{-2} \sum_{i=1}^{n} \xi_i (\vec{l}_i \cdot \vec{s}_i) \right| l^n v'L'S'M'_L M'_S \right\rangle \quad (16)$$

(d) the orbital Zeeman term

$$H_{IJ}^{\mathrm{lB}} = \left\langle l^n vLSM_L M_S \left| \hat{V}^{\mathrm{lB}} \right| l^n v'L'S'M'_L M'_S \right\rangle$$
$$= \delta_{v,v'}\delta_{L,L'}\delta_{S,S'}\delta_{M_S,M'_S} \left\langle l^n vLSM_L M_S \left| \hbar^{-1}\mu_{\mathrm{B}}\kappa(\vec{B}\cdot\vec{L}) \right| l^n v'L'S'M'_L M'_S \right\rangle \quad (17)$$

(e) the spin Zeeman term

$$H_{IJ}^{\mathrm{sB}} = \left\langle l^n vLSM_L M_S \left| \hat{V}^{\mathrm{sB}} \right| l^n v'L'S'M'_L M'_S \right\rangle$$
$$= \delta_{v,v'}\delta_{L,L'}\delta_{S,S'}\delta_{M_L,M'_L} \left\langle l^n vLSM_L M_S \left| \hbar^{-1}\mu_{\mathrm{B}} g_{\mathrm{e}} (\vec{B}\cdot\vec{S}) \right| l^n v'L'S'M'_L M'_S \right\rangle \quad (18)$$

Here, the Racah operator (rationalized spherical harmonics) $\hat{C}_q^k(i) = (4\pi/2k+1)^{1/2} Y_q^k(i)$ occurs; *k*–rank, *q*–component. The parameter

$$F_k(R_K) = \left(e^2/4\pi\varepsilon_0\right)\left\langle r_>^{-(k+1)} \cdot r_<^k \right\rangle \approx \left(e^2/4\pi\varepsilon_0\right) R_K^{-(k+1)} \cdot \left\langle r^k \right\rangle \quad (19)$$

refers to the crystal-field strength of the *K*-th ligand; $F_{ll}^k = \left(e^2/4\pi\varepsilon_0\right)\left\langle r_>^{-(k+1)} \cdot r_<^k \right\rangle$ are Slater-Condon parameters of rank *k*. The orbital Zeeman term includes *κ*–orbital reduction factor. The advantage of this approach is that all matrix elements can be expressed through closed formulae [18,19]. By selecting certain combination of operators/matrix elements, several cases can be mapped:

(i) By diagonalizing the matrix

$$H_{IJ} = H_{IJ}^{\mathrm{ee}} + H_{IJ}^{\mathrm{cf}} \quad (20)$$

the resulting eigenvalues refer to the energies of crystal-field terms. No constrain to the crystal-field strength is needed (weak field, strong field, intermediate field) since the variation principle is applied. The resulting eigenvectors $\left| l^n(vL)SM_S\Gamma\gamma a \right\rangle$ can be probed for symmetry operations of the respective point group of symmetry allowing a classification according to the irreducible representations Γγ (like A_{2g}, T_{1g}, T_{2g} for the group O_h of the d^8 system, Mulliken notation).

(ii) By diagonalizing the matrix

$$H_{IJ} = H_{IJ}^{\mathrm{ee}} + H_{IJ}^{\mathrm{cf}} + H_{IJ}^{\mathrm{so}} \quad (21)$$

one gets the crystal-field multiplets. The eigenvectors $\left| l^n(vLS)J\Gamma'\gamma' b \right\rangle$, when probed to symmetry operations of the respective double group, yield assignment of the Bethe symbols (Γ_1 through Γ_8 for the O′ double group) to the energy levels.

(iii) By diagonalizing the matrix

$$H_{IJ} = H_{IJ}^{\mathrm{ee}} + H_{IJ}^{\mathrm{cf}} + H_{IJ}^{\mathrm{so}} + H_{IJ}^{\mathrm{lB}}(B) + H_{IJ}^{\mathrm{sB}}(B) \quad (22)$$

Preprints (www.preprints.org) | NOT PEER-REVIEWED | Posted: 27 September 2023 doi:10.20944/preprints202309.1797.v1

the Zeeman levels dependent upon the magnetic field are obtained. They enter the partition function $Z(B,T)$ from which the magnetization components $M_\alpha(B,T)$, the susceptibility components $\chi_{ab}(B,T)$, and eventually the heat capacity $c_V(B,T)$ can be obtained by the apparatus of the statistical thermodynamics [18,19].

The above matrices, in general, are complex-Hermitian so that the programming requires complex*16 arithmetic. The size of the basis set for d^5 through d^9 systems is 256, 210, 120, 45, and 10 members, respectively. In this approach the configuration interaction is naturally involved and it is termed the Generalized Crystal-Field Theory (GCFT).

4. Zero-Field Splitting Parameters

The application of the spin-Hamiltonian offers a modelling of the energy levels, magnetization, and magnetic susceptibility depending upon the spin quantum number S = 1, 3/2, 2, and 5/2. The corresponding spin matrices have dimension of 3, 4, 5, and 6 in the basis set of spin kets $|S,M_S\rangle$. The members of the spin multiplets in the zero field are separated by amount D, $2D$, (D, $3D$) and ($2D$, $4D$), respectively as shown in Figure 1.

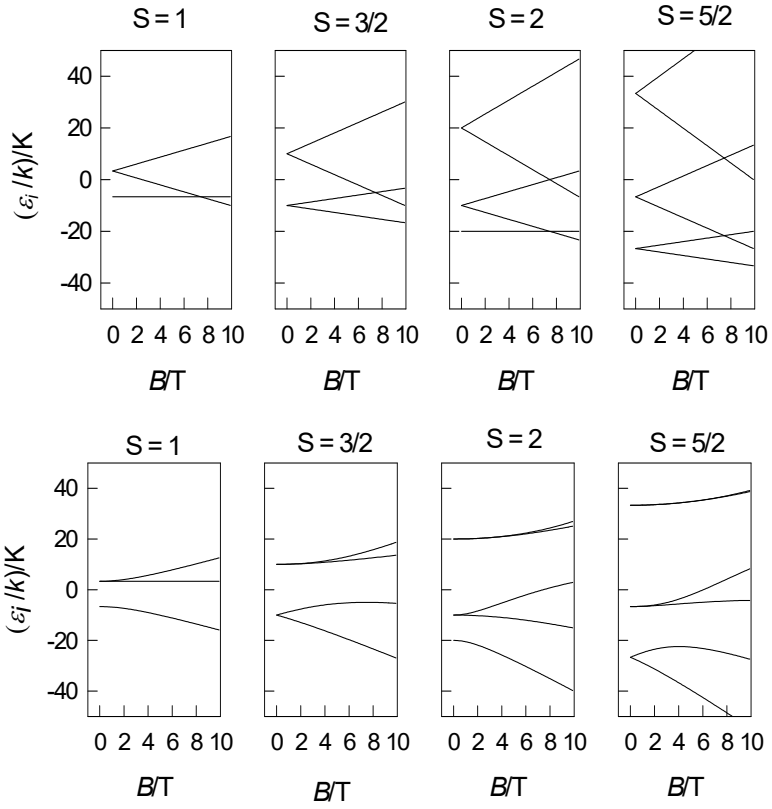

Figure 1. Energy levels modelled by the spin-Hamiltonian formalism, D/k = 10 K; parallel direction (z)-upper panel, perpendicular direction (x)–bottom panel.

In general, the spin Zeeman term depends upon the polar coordinates (ϑ,φ) as follows

$$\hat{H}^{Z}_{kl,m} = \mu_B B_m (g_x \sin\vartheta_k \cos\varphi_l \hat{S}_x + g_y \sin\vartheta_k \sin\varphi_l \hat{S}_y + g_z \cos\vartheta_k \hat{S}_z)\hbar^{-1} \quad (23)$$

where (k, l) refer to grids distributed uniformly over a sphere. In this way the magnetization can be visualized *via* a 3D-diagram as shown in Figure 2. It must be noted that when $|D| < 3E$, a renumbering of the Cartesian axes results to the usual constraint $|D| > 3E$. In a very high field (50 T) the system becomes isotropic and its 3D-magnetization refers to a sphere.

At the higher level of the theory (GCFT), when all members of the d^n configuration are considered, the D and E values are not rigorously defined. Figure 3 brings a modelling of the lowest

Preprints (www.preprints.org) | NOT PEER-REVIEWED | Posted: 27 September 2023 doi:10.20944/preprints202309.1797.v1

energy gap between crystal-field multiplets beyond the SH formalism by using GCFT for a wide range of the crystal-field strengths; it is briefly discussed below.

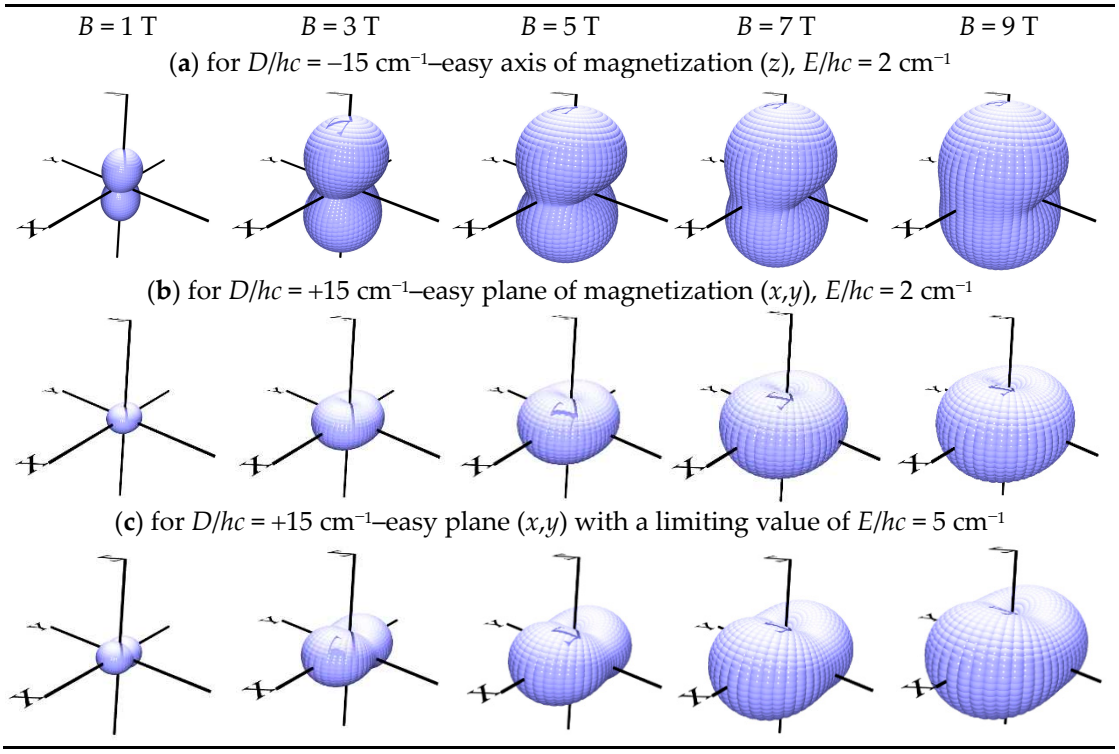

Figure 2. 3D-view of the magnetization $M(D,E)$ for different applied field, $S = 1$.

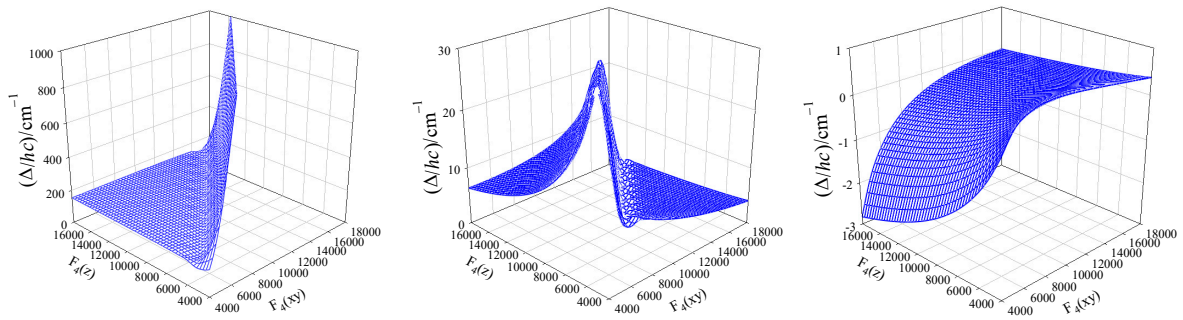

d¹, Ti(III), $^2T_{2g}$, no zfs

d², V(III), $^3T_{1g}$, zfs for compression

d³, Cr(III), $^4A_{2g}$, zfs

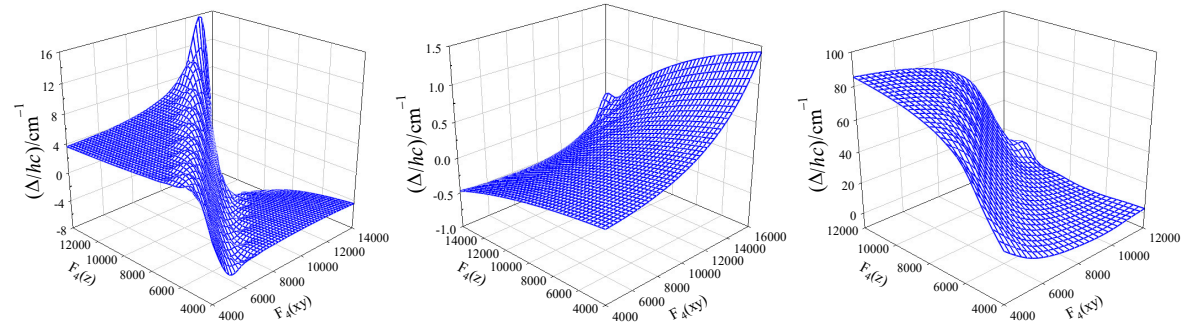

d⁴, Mn(III), ^5E_g

d⁵, Fe(III), $^6A_{1g}$, zfs

d⁶, Fe(II), $^5T_{2g}$, zfs for elongation

Preprints (www.preprints.org) | NOT PEER-REVIEWED | Posted: 27 September 2023 doi:10.20944/preprints202309.1797.v1

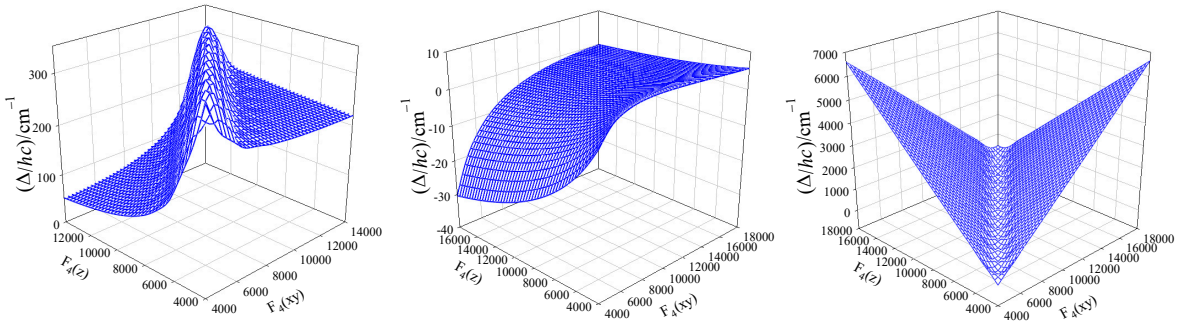

d^7, Co(II), $^4T_{1g}$, zfs for compression

d^8, Ni(II), $^3A_{2g}$, zfs

d^9, Cu(II), ^2E_g, no zfs

Figure 3. Calculated lowest energy gap by the GCFT over a wide range of the crystal-field strengths between compressed and elongated tetragonal bipyramid (D_{4h}) for the electron configurations d^1 through d^9. The *D*-parameter results from the splitting of a non-degenerate ground electronic term by the spin-orbit interaction.

The octahedral d^3 and d^8 systems are fortunate cases since the ground electronic term is nondegenerate ($^4A_{2g}$, $^3A_{2g}$) and it stays nondegenerate for the whole array of compressed and elongated tetragonal bipyramids ($^4B_{1g}$, $^3B_{1g}$). For Ni(II) complexes (S = 1) the lowest crystal-field multiplets, labelled in the D′$_4$ double group by Bethe (Mulliken) symbols $\Gamma_4(B_2)$ and $\Gamma_5(E_1)$ are separated by the energy gap $\Delta = \varepsilon(\Gamma_5) - \varepsilon(\Gamma_4)$; this value adopts role of the *D*-parameter (the Γ_5 level is doubly degenerate in the zero field). $D > 0$ applies for an elongated tetragonal bipyramid, and $D <$ 0 holds true for the compressed bipyramid. For the octahedral geometry the energy gap collapses to the zero. The range of *D*-values for Cr(III) is by one order of magnitude lower relative to Ni(II); this is a consequence of much lower spin-orbit splitting parameter λ/hc = 92 *vs* 315 cm^{-1} ($D \sim \lambda^2$).

The octahedral d^7 system possesses the ground term $^4T_{1g}$ that is orbitally triply degenerate. On distortion to a compressed tetragonal bipyramid it is split into {$^4A_{2g}$, ^4E_g} terms; on distortion to an elongated bipyramid the splitting is opposite {^4E_g, $^4A_{2g}$}. The spin-orbit coupling causes a further splitting to six Kramers doublets: $1\Gamma_6$, $1\Gamma_7$, $2\Gamma_6$, $3\Gamma_6$, $2\Gamma_7$, $3\Gamma_7$ for the compression and $1\Gamma_6$, $2\Gamma_6$, $1\Gamma_7$, $2\Gamma_7$, $3\Gamma_6$, $3\Gamma_7$ for the elongation. This means that only the first case is consistent with the SH formalism and, moreover, the crystal field asymmetry should be large (much stronger axial crystal field $F_4(z)$); in such a case always $\Delta = 2D > 0$ and it is very high (typically 200 cm^{-1}).

The counter parting d^2 system with the ground state $^3T_{1g}$ resembles the tetragonal splitting to {$^3A_{2g}$, ^3E_g} on the compression and the spin-orbit coupling splits the ground term into $\Gamma_1(A_1)$ and $\Gamma_5(E_1)$ multiplets. In this case $\Delta = D > 0$ holds true. For the elongated bipyramid the six-membered multiplet manifold is $\Gamma_3(B_1)$, $\Gamma_4(B_2)$, $\Gamma_5(E_1)$, $\Gamma_1(A_1)$, $\Gamma_2(A_2)$ and it has no relationship to the SH approach.

For Mn(III) systems (d^4, S = 2) the situation is more complex. The spin-Hamiltonian (SH) formalism predicts that for $D > 0$ (compressed tetragonal bipyramid) the ground state $|S, M_S\rangle$ is a singlet $|2,0\rangle$; the first excited Kramer doublet $|2,\pm1\rangle$ is by the *D*-value higher, and the second excited Kramer doublet $|2,\pm2\rangle$ lies by 4*D* amount above the ground state. The GCFT is consistent with SH-formalism only for the first three multiplets Γ_1 and Γ_5 (doubly degenerate). The remaining two excited states Γ_3 and Γ_4 are not exactly degenerate (they do not form a Kramer doublet) but they are split in the zero field by 0.2 cm^{-1}. (Calculated energy levels are, for instance: $\Gamma_1(A_1)\times1$ at 0; $\Gamma_5(E_1)\times2$ at 5.1 cm^{-1}; $\Gamma_3(B_1)\times1$ at 19.8 cm^{-1}; $\Gamma_4(B_2)\times1$ at 20.0 cm^{-1}. Thus, for D = 5.1 cm^{-1} is 4*D* = 20.4 cm^{-1}, but the Γ_4 level is by 0.4 cm^{-1} lower.) This demonstrates that we cannot rely to the spin-Hamiltonian formalism in all cases.

The d^6 system, like high-spin Fe(II), again is a complex task. In the octahedral geometry the ground term is orbitally triply degenerate, $^5T_{2g}$. On tetragonal elongation it is split to {$^5B_{2g}$, ^5E_g} terms and five member of the ground term $^5B_{2g}$ are further split by the spin-orbit interaction into multiplets Γ_4, Γ_5, Γ_1, Γ_2. Then the SH formalism is approximately valid (the Γ_1, Γ_2 pair is quasi-degenerate and separated from the ground Γ_4 by *ca* 4*D*); *D*-value is moderate: $D/hc \sim 10$ cm^{-1}. On tetragonal

Preprints (www.preprints.org) | NOT PEER-REVIEWED | Posted: 27 September 2023 doi:10.20944/preprints202309.1797.v1

compression the 10-membered manifold of the ^5E_g term is split in the way having no relationship to the SH formalism, so that the *D*-parameter is undefined.

The electronic structure of tetrahedral d^n systems matches complementary octahedral systems d^{10-n}. For instance, tetrahedral Co(II)–d^7 possesses the ground state $^4A_2$, like octahedral Cr(III)–d^3.

5. Magnetostructural J-Correlations

Before proceeding to the discussion of magnetostructural D-correlations, we briefly mention the original type of correlation analysis of structure-magnetism relations in transition metal complexes. Relationships between selected structural parameters and the magnetic properties of dinuclear (polynuclear) metal complexes were outlined by Hatfield [20,21], his co-workers and followers. In the [Cu^{II}-$(OH)_2$-Cu^{II}] type complexes the isotropic exchange constant *J* correlates with the bond angle α = Cu-O-Cu along a straight line with negative slope

$$J[\mathrm{cm}^{-1}] = -74.53\cdot\alpha[^\circ] + 7270,\ r = -0.99 \tag{24}$$

Involvement of more data with greater structural diversity along the superexchange path led to the differentiation according to the alkoxido- or phenoxido- class [22]. Analogous linear correlations were developed for [Cr^{III}-$(OH)_2$-Cr^{III}] and [Mn^{IV}-$(O)_2$-Mn^{IV}] type complexes [23–25].

According to Gorun and Lippard the *J*-value correlates with the shortest Fe-O distance (abbr. *P*) along the superexchange path in the [Fe^{III}-O-Fe^{III}] type complexes [26]. The correlation was proposed along a decreasing exponential curve that is applicable only in the segment of negative *J*

$$-J[\mathrm{cm}^{-1}] = (2.360\times10^{10})\cdot\exp(-10.661\ P[10^{-10}\ \mathrm{m}]),\ r = -0.97 \tag{25}$$

However, also a linear correlation is acceptable, hence [27]

$$J[\mathrm{cm}^{-1}] = 525.7\cdot P[10^{-10}\ \mathrm{m}] - 1055,\ r = 0.96 \tag{26}$$

It must be critically said that any kind of magnetostructural relationship or correlation heavily depends upon the quality of structural and magnetic data. Another aspect is that almost all correlations are restricted to the linear relationships of *J*-α or *J*-*P* type. Nowadays, modern packages of statistical software (multivariate methods) are at the disposal: correlation analysis, Cluster Analysis, Principal Component Analysis, Factor Analysis, etc. can be applied to the carefully filtered datasets. An approach like this appeared very recently [28,29].

6. Magnetostructural D-Correlations

It is obvious that, the correlation *D vs P* (a geometrical parameter) is derived from the electronic structure of complexes. The problem of electronic structure, as well as magnetic properties, is solved mainly at the level of quantum-chemical (first principle) calculations [79–81]. Application of the partitioning technique and/or quasi-degenerate perturbation theory yields the matrix elements of the effective Hamiltonian spanned by the spin manifold of the orbitally non-degenerate ground electronic state $|0SM\rangle$ as follows

$$\begin{aligned}\left\langle 0SM\left|\hat{H}_{\mathrm{eff}}\right|0SM'\right\rangle &= E_0\delta_{MM'} + \left\langle 0SM\left|\hat{H}_1\right|0SM'\right\rangle \\ &- \sum_{bS''M''}\Delta_b^{-1}\left\langle 0SM\left|\hat{H}_1\right|bS''M''\right\rangle\cdot\left\langle bS''M''\left|\hat{H}_1\right|0SM'\right\rangle\end{aligned} \tag{27}$$

with the denominator defined by excitation energies

$$\Delta_b^{-1} = (E_b - E_0)^{-1},\quad E_0 = \left\langle 0SM\left|\hat{H}_0\right|0SM\right\rangle \tag{28}$$

Then the D-tensor components (m, $n = x, y, z$) arising from the spin-orbit interaction are obtained in the form

Preprints (www.preprints.org) | NOT PEER-REVIEWED | Posted: 27 September 2023 doi:10.20944/preprints202309.1797.v1

$$D_{mn}^{(0)} = -\frac{1}{S^2}\sum_{b(S_b=S)}\Delta_b^{-1}\left\langle 0SS\left|\sum_i \hat{h}_m^{(i)}\hat{s}_z^{(i)}\right|bSS\right\rangle \cdot\left\langle bSS\left|\sum_i \hat{h}_n^{(i)}\hat{s}_z^{(i)}\right|0SS\right\rangle \quad (29)$$

$$D_{mn}^{(-1)} = -\frac{1}{S(2S-1)}\sum_{b(S_b=S-1)}\Delta_b^{-1}\left\langle 0SS\left|\sum_i \hat{h}_m^{(i)}\hat{s}_{+1}^{(i)}\right|b,S-1,S-1\right\rangle \cdot\left\langle b,S-1,S-1\left|\sum_i \hat{h}_n^{(i)}\hat{s}_{-1}^{(i)}\right|0SS\right\rangle \quad (30)$$

$$D_{mn}^{(+1)} = -\frac{1}{(S+1)(2S+1)}\sum_{b(S_b=S+1)}\Delta_b^{-1}\left\langle 0SS\left|\sum_i \hat{h}_m^{(i)}\hat{s}_{-1}^{(i)}\right|b,S+1,S+1\right\rangle \cdot\left\langle b,S+1,S+1\left|\sum_i \hat{h}_n^{(i)}\hat{s}_{+1}^{(i)}\right|0SS\right\rangle \quad (31)$$

where the one-electron (i) orbital operator for the spin-orbit coupling is

$$\hat{h}_m^{(i)} = \sum_A \xi_A^{(i)}\hat{l}_{mA}^{(i)} \quad (32)$$

A comparison with the simple perturbation theory applied to the crystal-field terms arising from d-electrons of the central atom [82–84]

$$D_{mn}^{\mathrm{CFT}} = -\frac{1}{4S^2}\sum_{K\neq 0}\frac{\left\langle 0\left|\hat{L}_m\xi\right|K\right\rangle\left\langle K\left|\hat{L}_n\xi\right|0\right\rangle\hbar^{-2}}{E_K - E_0} \quad (33)$$

shows that more contributions are in the play. Quantum-chemical calculations show that the individual contributions to the D-parameter are different in size and sign and a lot of terms approximately cancel. The dominating part arises from the spin-orbit coupling, however, the contributions from the spin-spin interaction also cannot be completely neglected in many cases [85].

A much simplified approach is GCFT. By inspecting Figure 4 it is possible to transform the 3D-graph $D = f(F_4(xy), F_4(z))$ into a 2D-diagram $D = f(P)$. The crystal-field poles can be expressed through the fourth electronic moment $<r^4>$ common for the complex as follows

$$F_4(R_K) \approx \left(e^2 / 4\pi\varepsilon_0\right)R_K^{-5}\left\langle r^4\right\rangle \quad (34)$$

hence a relationship

$$\left(e^2 / 4\pi\varepsilon_0\right)\left\langle r^4\right\rangle = F_4(z)R_z^5 = F_4(xy)R_{xy}^5 \quad (35)$$

holds true. This method enables relatively fast mapping of structural dependence of the D-parameter for a wide range of distortions.

6.1. Hexacoordinate Ni(II) Complexes

Magneto-structural relationships for the nearly-octahedral Ni(II) complexes was mapped along tetragonal distortion mode characterized by the difference between axial (R_z) and equatorial (R_{xy}) metal-ligand bond lengths. Thus, the structural D-parameter can be expressed by introducing the X_F function as follows

$$D_{\mathrm{str}} = R_z - R_{xy} = R_z\left[1-\left(\frac{F_4(z)}{F_4(xy)}\right)^{1/5}\right] = R_z \cdot X_F \quad (36)$$

Preprints (www.preprints.org) | NOT PEER-REVIEWED | Posted: 27 September 2023 doi:10.20944/preprints202309.1797.v1

A modelling of the magnetic *D*-values (exact multiplet splitting) depending upon the transformed structural ordinate is shown in Figure 4. Important message is that such dependence is generally non-linear; however, within the relevant experimental range it follows a nearly linear relationship. In fact, the dependence–the correlation line of the magnetostructural D-correlation is represented by a pair of nearly collinear straight lines intercepting at the octahedral geometry where D and D_{str} are zero. The calculations by GCFT were done for the nephelauxetic ratio $\beta = 1$, and the orbital reduction factors $\kappa_z = \kappa_{xy} = 1$; therefore, the results are tentative.

The magnetic data used hereafter were collected quite recently using the SQUID magnetometer. The magnetic susceptibility (χ) was taken at the applied field of $B_{DC} = 0.1$ T between $T = 1.9$ and 300 K. The magnetization data (M) was taken at $T = 2.0$ and 4.6 K respectively, up to $B = 5$ or 7 T. Both datasets were fitted simultaneously by a numerical procedure that minimizes a joint functional $F = R(\chi) \cdot R(M)$. A collection of 25 data-points is displayed in Figure 5 along with a common (linear) correlation curve passing through the origin: $D[\mathrm{cm}^{-1}] = 0.632 \cdot D_{str}[\mathrm{pm}]$. The list of the compounds and numerical data is collected in Supplementary Information [30–37]. The correlation predicts that with increasing structural tetragonality D_{str} (in the direction compressed tetragonal bipyramid–octahedron–elongated tetragonal bipyramid) the axial zero-field splitting parameter D increases.

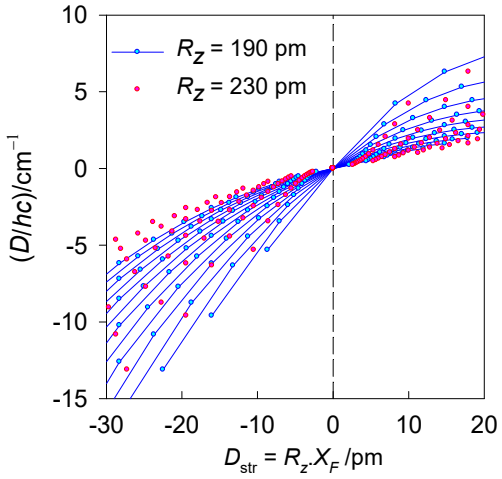

Figure 4. Calculated magnetic *D*-values (exact multiplet splitting by GCFT) for different equatorial-axial crystal-field strengths *vs* the transformed structural ordinate D_{str} for hexacoordinate Ni(II) complexes. Solid lines interpolate the points for common axial metal-ligand distance $R_z = 190$ pm. Red points bracket the second limiting case, $R_z = 230$ pm.

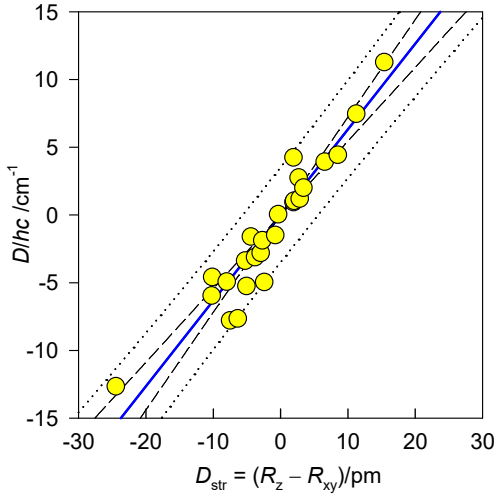

Figure 5. Magnetostructural D-correlation for hexacoordinate Ni(II) complexes. Confidence and prediction intervals are shown at 95 % probability level.

Preprints (www.preprints.org) | NOT PEER-REVIEWED | Posted: 27 September 2023 doi:10.20944/preprints202309.1797.v1

It must be mentioned that for the complexes with a heterogeneous coordination sphere, e.g., possessing {NiN_4O_2} chromophore, the evaluation of the experimental value of D_{str} requires a correction taking into account the averaged bond lengths of the given donor atom. For instance

$$D_{str} = \Delta_z - (\Delta_y + \Delta_x)/2 \quad (37)$$

where $\Delta_a = (R_a - \bar{R}_a)$ for $a = x, y, z$ is a shift relative to the mean distance $\bar{R}_a$ for a given bond. For the N- and O-donor ligands these values have been taken from complexes containing the $[Ni(NH_3)_6]^{2+}$ and $[Ni(H_2O)_6]^{2+}$ units, respectively: $\bar{R}(Ni-N) =$ 2.145 and $\bar{R}(Ni-O) =$ 2.055 Å. For a more ionic bond the value of $\bar{R}(Ni-NCS) =$ 2.070 Å was used.

Another piece of information brings the Principal Component Analysis (PCA) which transforms the set of original variables to their linear combinations (principal components) bearing the maximum variability of the data. Two components bear 94.7 % of the variability in the present case. The biplot in Figure 6 shows how the individual variables are interrelated: the closest rays refer to a positive correlation, the farthest to a negative one (anticorrelation). The graph proves that the g-factor asymmetry (gdif = $g_z - g_{xy}$) anticorrelates with the D parameter in agreement with the spin-Hamiltonian formula $D = -(\xi/2S)(g_z - g_{xy})/2$. Classification of the individual points according to the clusters allows us to visualize the clusters separation.

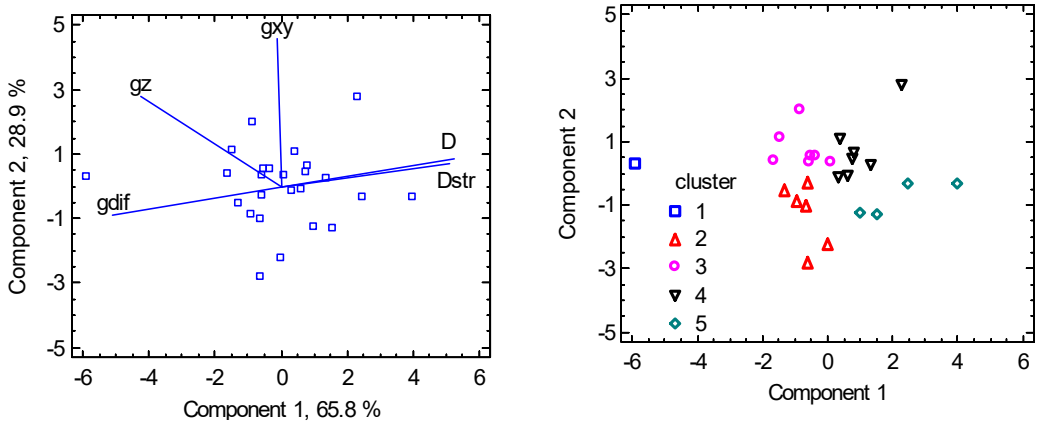

Figure 6. PCA biplot for hexacoordinate Ni(II) complexes. The points are the individual objects.

The Factor Analysis (FA) constructs a small number of new variables–common factors which represent a large percentage of the variability in the original variables. Factor loadings may be obtained from either the sample covariance or sample correlation matrix. The initial loadings may be rotated (e.g., by varimax rotation). Two factors cover 96.5 % of the variability of the original data (D_{str}, D, g_{xy}, and g_z) in the present case (Figure S1). Again, the strong correlation of parameters D and D_{str} is confirmed.

6.2. Hexacoordinate Co(II) Complexes

The above procedure outlined for Ni(II) complexes has been also applied to a set of hexacoordinate Co(II) complexes. As already mentioned, only the segment of the compressed tetragonal bipyramids matches the spin-Hamiltonian formalism and the D-values are expected to be very high [38–48].

A collection of 16 data-points is displayed in Figure 7 (left) from which it is evident that a linear correlation does not apply in this case. This is understood from the transformed 3D-graph $D = f(F_4(xy), F_4(z))$ to a 2D-diagram $D = f(D_{str})$ (Figure 7, right). For the complexes with a heterogeneous coordination sphere the mean distances $\bar{R}(Co-N) =$ 2.185, $\bar{R}(Co-O) =$ 2.085, and $\bar{R}(Co-Cl) =$ 2.475 Å were used in calculating experimental D_{str} values. The data worksheet is listed in SI and processed by the multivariate statistical methods. The Cluster Analysis based upon three variables (labelled as Dstr, D2 = 2D and gxy) shows that the distance separates the objects into two principal clusters (Figure 8). Their separation is well seen also from the Principal Component Analysis (Figure S2). The assumption on which the correlation 2D *vs* D_{str} is based is thus statistically confirmed.

Preprints (www.preprints.org) | NOT PEER-REVIEWED | Posted: 27 September 2023 doi:10.20944/preprints202309.1797.v1

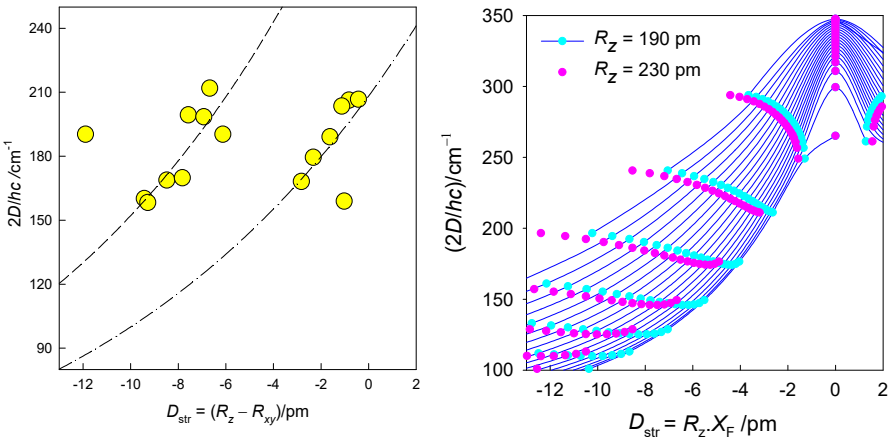

Figure 7. Magnetostructural D-correlation for hexacoordinate Co(II) complexes. Lines–fitted with an exponential, $2D = b \cdot \exp(c \cdot D_{str})$ (**left**). Calculated magnetic *D*-values for different equatorial-axial crystal-field strengths *vs* the transformed structural ordinate D_{str} for hexacoordinate Co(II) complexes. Solid lines interpolate the points for common axial metal-ligand distance R_z = 190 pm. Red points bracket the second limiting case, R_z = 230 pm (**right**).

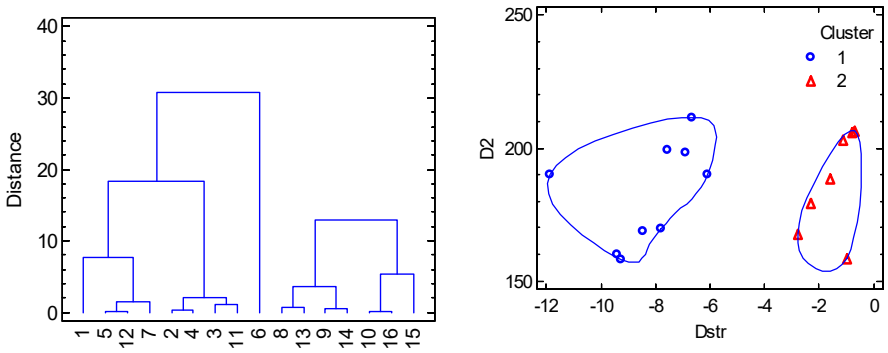

Figure 8. Cluster analysis for hexacoordinate Co(II) complexes. Individual cluster areas are circled.

6.3. Tetracoordinate Co(II) Complexes

A collection of the spin-Hamiltonian parameters in this case is based upon High-Frequency/High-Field Electron Spin Resonance (syn. EPR, EMR)–10 datapoints, and completed by 5 results from a simultaneous fitting of the susceptibility/magnetization data for [CoA_2B_2] type complexes [49–54]. The basic problem arises from the fact that in addition to radial variations (bond lengths Co-A, Co-B) also the angular distortion (bond angles A-Co-A, B-Co-B) is substantial. Moreover, four twisting angles A-Co-B come into the play (in total, 9 coordinates are independent).

The importance of the angular distortion was proven by modelling using the GCFT that is shown in Figure 9; the energy gap between the lowest crystal-field multiplets refers to $\Delta = 2(D^2 + 3E^2)^{1/2} \doteq 2D$. On right, the transformed ordinate was used for the 2D plot giving rise to a general route to be followed by the magnetostructural D-correlation in tetracoordinate Co(II) complexes. It proceeds according to an increasing exponential. The correlation of *D vs* A_- is shown in Figure 10 and it can be concluded that the experimental data matches the general course predicted by GCFT modelling. A fit to exponential curves $D = a + b \cdot \exp(c \cdot A\_)$ is also shown by dashed lines.

Preprints (www.preprints.org) | NOT PEER-REVIEWED | Posted: 27 September 2023 doi:10.20944/preprints202309.1797.v1

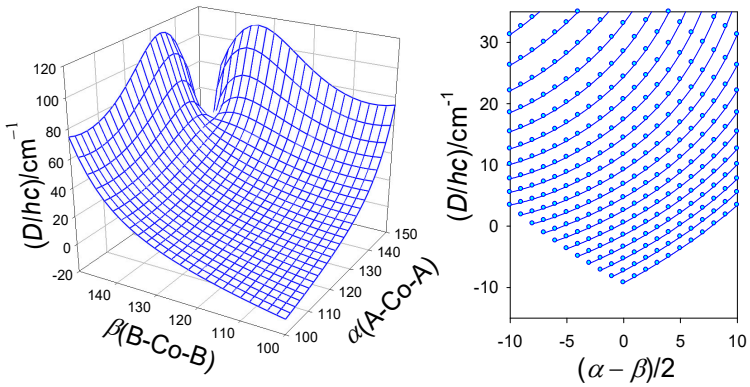

Figure 9. Calculated magnetic *D*-values (exact multiplet splitting by GCFT) for different distortion angles α (A-Co-A) and β (B-Co-B) (in deg) with fixed crystal-field strengths $F_4(R)$ = 5000 cm^{-1}. Right–transformed 2D graph for increasing angle α (from **bottom** to **top**).

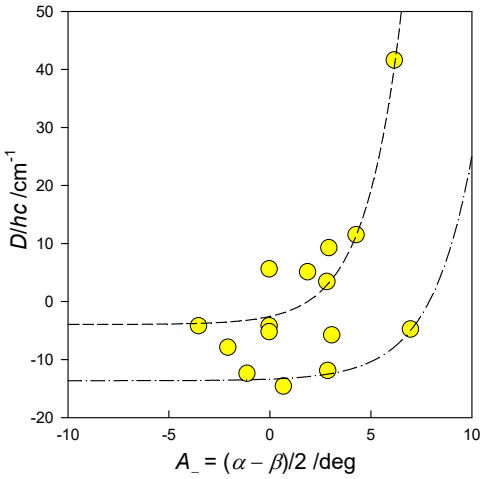

Figure 10. Magnetostructural D-correlation for tetracoordinate Co(II) complexes.

For the multivariate methods, 7 variables were considered: *R*(Co-A), *R*(Co-B), α(A-Co-A), β(B-Co-B), g_z, g_{xy}, *D* abbreviated as RA, RB, alpha, beta, gz, gxy, D. Also, three transformed variables were added: Aplus = (alpha + beta)/2, Aminus = (alpha–beta)/2, gdif = gz–gxy. It must be mentioned that the data involve very different chromophores as follows: {CoN_4}, {CoN_2N_2}, {$CoCl_4$}, {$CoBr_4$}, {$CoCl_2P_2$}, {$CoBr_2P_2$}, and the most numerous {$CoCl_2N_2$} one. (Two datapoints with {CoN_2O_2}, {CoO_2S_2} chromophores were deleted from consideration due to evident dissimilarity). The Cluster Analysis points to two principal clusters (Figure 11) containing 11 and 4 members, respectively. Eventually, the compound with large D/hc = 41 cm^{-1} could be classified as a new cluster. The PCA method (Figure 12) shows a rather weak correlation of the *D*-values with individual geometric parameters; the best correlation is D *vs* Aminus. PCA also confirms an anticorrelation of D and gdif as expected by the spin-Hamiltonian formalism. On the other hand, the PCA analysis evidently separates the individual clusters.

Preprints (www.preprints.org) | NOT PEER-REVIEWED | Posted: 27 September 2023 doi:10.20944/preprints202309.1797.v1

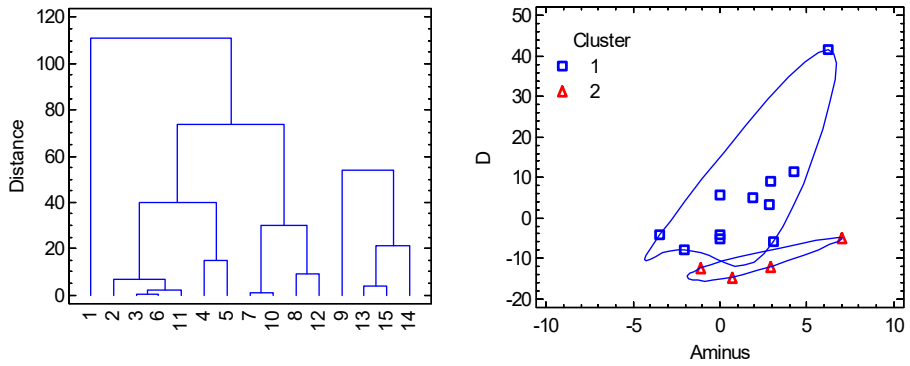

Figure 11. Cluster analysis for tetracoordinate Co(II) complexes. Individual cluster areas are circled.

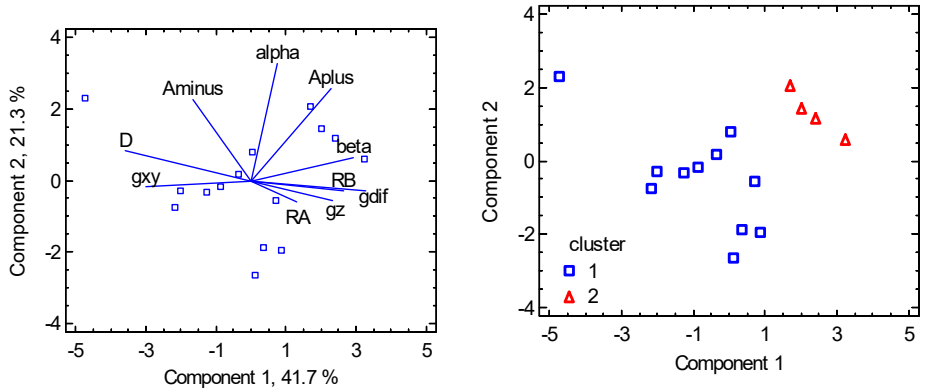

Figure 12. PCA biplot for tetracoordinate Co(II) complexes. The points are the individual objects.

6.4. Pentacoordinate Co(II) Complexes

For pentacoordinate complexes of the [$CoXA_2B_2$] type the basic obstacle arises from the fact that too many (12) geometrical parameter come into the play and the coordination polyhedron is often far from the ideal tetragonal pyramid and/or trigonal bipyramid. Also the description of the intermediate geometries through the angular distortion (trigonality) τ-parameter represents a strong idealization. Moreover, there are only a few reliable magnetic data based upon both, the susceptibility and magnetization measurements (HF/HF EPR cannot be used since *D*-values are too large).

The angular dependence of the *D*-parameter with respect to two geometrical parameters is shown in Figure 13: polar angles θ(A) and θ(B) were used in mapping the Berry-kind of transformation between trigonal bipyramid and tetragonal pyramid using GCFT. Worth noting is the fact that majority of the complexes under study possess trigonality parameter $\tau > 1$ due to a rigid tridentate ligand with the {XA_2} donor set.

Eleven datapoints have been collected (see SI) [55–59] and the variables *R*(Co-X), *R*(Co-A), *R*(Co-B), α(A-Co-A), β(B-Co-B), θ(X-Co-A), θ(X-Co-B), *D*, g_{xy} are abbreviated for statistical analysis as RX, RA, RB, alpha, beta, thetaA, thetaB, D, gxy. Moreover, three transformed variables were considered: $\gamma = 360–2\theta$(A), $\tau = (\alpha - \beta)/60$ or $\tau = (\gamma–\beta)/60$ when $\gamma > 180$ deg, and $\delta = (\alpha–\beta)/2$ abbreviated as gamma, tau and dis. The cluster analysis distinguishes two main clusters with 8 and 3 datapoints, respectively (Figure 14). For the first cluster $\gamma > 180$ deg and $\tau > 1$ holds true; for the second cluster: $\gamma < 180$ deg, $\tau < 1$. The PCA revealed a significant correlation of parameter *D* with parameters *R*(Co-X), *R*(Co-B), and g_x, which, however, does not provide more fundamental information in this case. Rather, a weak positive correlation with the γ parameter and anticorrelation with α appear to be more significant. Moreover, PCA again separates visibly two clusters (Figure 15).

Preprints (www.preprints.org) | NOT PEER-REVIEWED | Posted: 27 September 2023 doi:10.20944/preprints202309.1797.v1

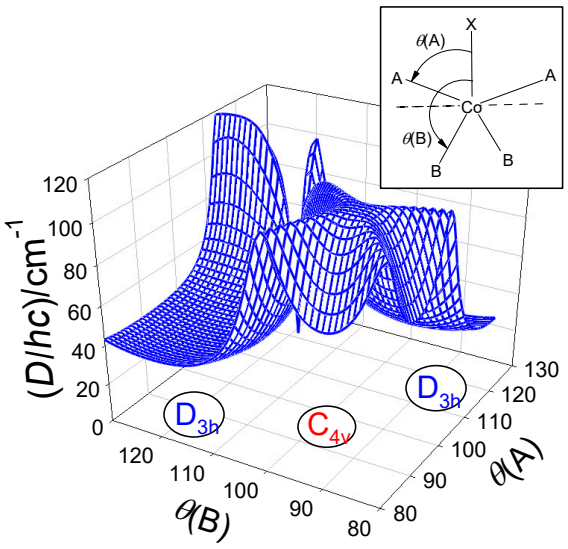

Figure 13. Calculated magnetic *D*-values (exact multiplet splitting by GCFT) for polar angles θ(A) and θ(B) (in deg) with fixed crystal-field strengths $F_4(R)$ = 6000 cm^{-1}.

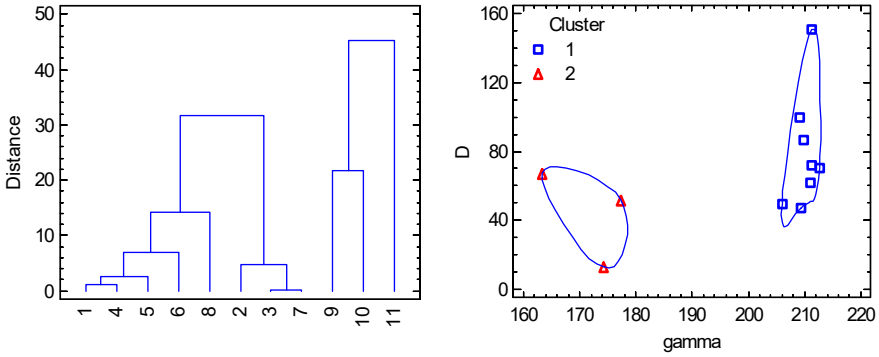

Figure 14. Cluster analysis for pentacoordinate Co(II) complexes. Individual cluster areas are circled.

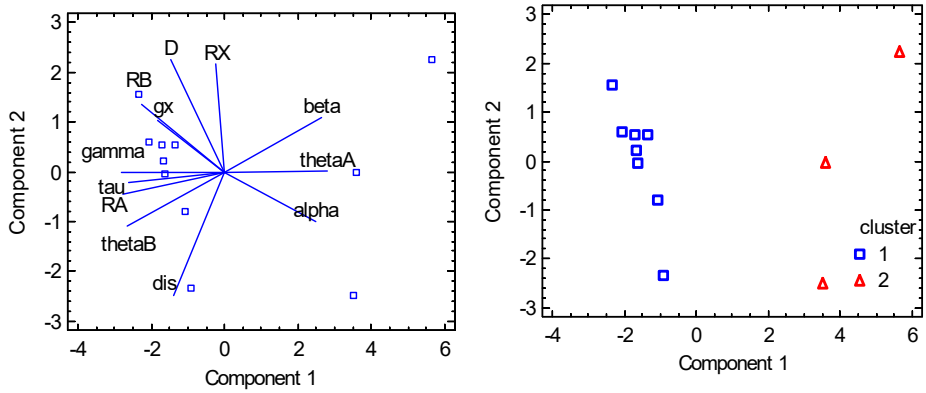

Figure 15. PCA biplot for pentacoordinate Co(II) complexes. The points are the individual objects.

A trial set of functions to fit the observed *D vs* structural parameter relationships is probed in Figure 16. Notice, the actual geometry is far from an ideal polyhedron where a crude averaging of bond angles was applied. Moreover, some of the [Co(L^{Cn})Cl$_2$] systems form a supramolecular dimer with exchange interaction $J > 0$. In such a case the local *D*-tensors are not necessarily collinear and this circumstance affects the fitted *D*-values. The correlation coefficient between *D* and g_x (r = 0.83) proves that the spin-Hamiltonian formula $D = \lambda(g_z - g_x)/2$ is fulfilled for pentacoordinate complexes.

Preprints (www.preprints.org) | NOT PEER-REVIEWED | Posted: 27 September 2023 doi:10.20944/preprints202309.1797.v1

This conclusion matches the forecast that only $D > 0$ applies for pentacoordinate Co(II) complexes [18,78]. In this light the reported values of D/hc= –40 cm^{-1} in {CoN_2N_3} type complexes seem be problematic: the authors fail in fitting the magnetization data and, moreover, they used closed formula for addition of three Cartesian components and neither their average nor a correct powder average was applied [74].

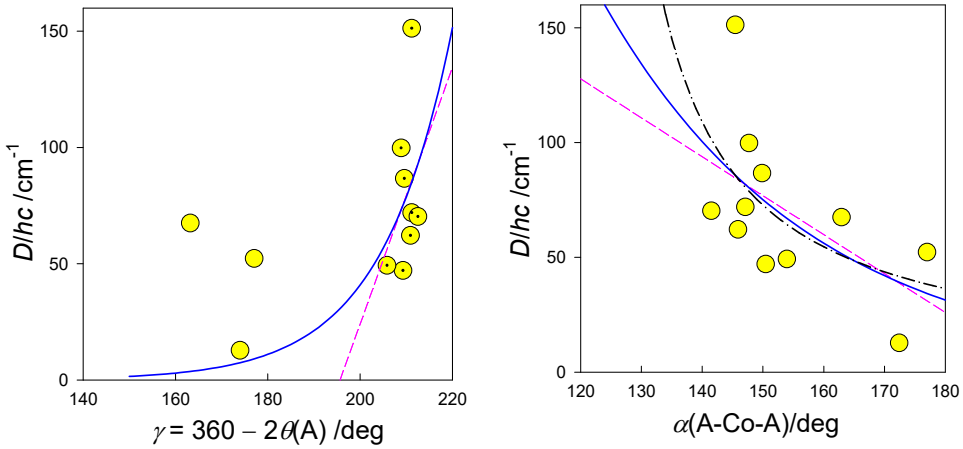

Figure 16. Magnetostructural D-correlation for pentacoordinate Co(II) complexes. Trial correlation curves: dashed–linear, solid–exponential $y = a \cdot \exp(bx)$, dot-dashed $y = y_0 + a / (x - x_0)$.

7. Selected Single-Molecule Magnets

List of known single-molecule magnets based upon one metal centre (single-ion magnets, SIM) is rapidly increasing. They cover, for instance, Mn(III), Mn(II), Fe(III), Fe(II), Fe(I), Co(II), Ni(III) and Ni(II) complexes) [60–77]. Representative examples for Co(II) are presented in Table 1. Worth noting is also an inverse relationship between the extrapolated relaxation time $\ln\tau_0$ and barrier to spin reversal U as shown in Figure 17.

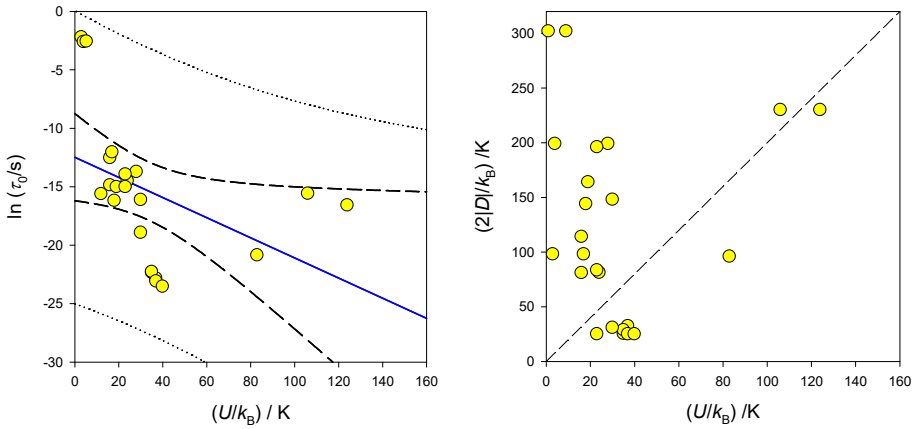

Figure 17. A relationship between the barrier to spin reversal and the extrapolated relaxation time in SIM containing Co(II). Right–interrelation of D and U (dashed–expected $U = 2|D|$).

The existence of the barrier to spin reversal is traditionally expected only for $D < 0$ (easy-axis of magnetization). However, SMM (SIM) behaviour was registered also in the case of $D > 0$; a presence of sufficient rhombic anisotropy ($E > 0$) rationalizes this observation. In this case, the easy-plane allowing unhindered relaxation no longer exists; small barrier to spin reversal is determined by the E parameter.

The above outlined magnetostructural correlations allows us to predict whether the system under study is a potential candidate for the single-molecule magnetism. For instance, observed value

Preprints (www.preprints.org) | NOT PEER-REVIEWED | Posted: 27 September 2023 doi:10.20944/preprints202309.1797.v1

of D/hc = –12.5 cm^{-1} in [Co(PPh$_3$)$_2$Br$_2$] complex from the DC magnetization studies motivated the AC susceptibility measurements and indeed, the SMM behaviour was confirmed [73].

Table 1. List of single-molecule (single-ion) magnets containing Co(II).

C.n.	Chromophore	Geometry [a]	(D/hc)/cm^{-1}	(E/hc)/cm^{-1}	B_{DC}/T	(U/k_B)/K	τ_0/s	Ref.
3	{CoN$_3$}		-57	12.7	0.08	16	3.5×10^{-7}	[69]
	{CoN$_2$O}		-72	13.5	0.06	18	9.3×10^{-8}	[69]
	{CoN$_2$P}		-82		0.075	19	3.0×10^{-7}	[69]
4	{CoS$_4$}		-74		0.10	30	1.0×10^{-7}	[70]
	{CoN$_3$Cl}		+12.7	1.2	0.15	35	2×10^{-10}	[71]
	{CoP$_2$Cl$_2$}		-16.2	0.9	0.10	37	1.2×10^{-10}	[72]
	{CoP$_2$Cl$_2$}		-14.4	1.7	0.10	35	2.1×10^{-10}	[72]
	{CoP$_2$Cl$_2$}		-15.4	1.3	0.10	30	6.0×10^{-9}	[72]
	{CoP$_2$Br$_2$}		-12.5		0.10	37	9.4×10^{-11}	[73]
					0.20	40	6.0×10^{-11}	[73]
5	{CoN$_3$N$_2$}	4py	-40.5	$J > 0$	0.20	16	3.6×10^{-6}	[74]
	{CoN$_3$N$_2$}	4py	-40.6		0.20	24	5.1×10^{-7}	[74]
	{CoN$_3$N$_2$}	3bpy	(+49.0), calc		0.06	17	5.85×10^{-6}	[59]
					0.56	3	0.110	[59]
	{CoN$_3$Cl$_2$}	4py	(+99.5), calc		0.06	28	1.1×10^{-6}	[59]
					0.56	4	0.074	[59]
	{CoN$_3$Cl$_2$}$_2$	4py	151	11.6, $J > 0$	0.20	9	3.1×10^{-7}	[58]
					0.20	1	0.27	[58]
6	{CoN$_4$N$_2$}		+48	13.0	0.30	83	8.7×10^{-10}	[48]
	{CoN$_4$N$_2$}		+98	8.4	0.10	23	3.0×10^{-7}	[75]
	{CoO$_3$N$_3$}		+41.7	1.6	0.10	23	8.9×10^{-7}	[76]
	{CoO$_6$}		-115	2.8	0	106	1.7×10^{-7}	[77]
					0.15	124	6.3×10^{-8}	[77]

[a] C.n.–coordination number; 4py–tetragonal pyramid, 3bpy–trigonal bipyramid; calc–estimate from the calculated energy gap between the lowest Kramers doublets as $\Delta = 2(D^2 + 3E^2)^{1/2} \sim 2D$.

The expected relationship for the half-integral spin S = 3/2 is $U = 2|D_S|$ (in the zero field) and this is evidently not obeyed (Figure 17). Questionable is also the way of extracting the SMM parameters: usually they arise from the Arrhenius-like linear relationship $\ln\tau = \ln\tau_0 + (U/k_B)T^{-1}$ applied to higher-temperature points. However, a more complex equation that involves also the Raman, direct and quantum tunnelling processes is available

$$\tau^{-1} = \tau_0^{-1}\exp(-U/k_BT) + CT^n + AB^2T + D(B) \quad (38)$$

This can be enriched by the phonon bottleneck effect FT^2 and the reciprocating thermal behaviour term GT^{-1}.

Some samples exhibit multiple relaxation processes that vary with the applied magnetic field so that it is problematic to relate single D with different U-values. Presence of various relaxation processes is visible only if a search for them was applied, e.g., for low (ν< 1 Hz) or high (ν> 1500 Hz) frequencies of the AC field. Co(II) complexes represent a rich class of single-ion magnets. These exhibit large magnetic anisotropy that for compressed tetragonal bipyramid necessarily is positive. The Orbach relaxation mechanism, however, required D < 0. For (pseudo)octahedral systems we found that the ZFS parameter D, and thus magnetic anisotropy, strongly decreases with tetragonal distortion. For near-octahedral structures, the D-parameter achieves large positive values (up to 350 cm^{-1} for ideal O$_h$–Jahn-Teller systems). Hexacoordinate Co(II) complexes with markedly negative D values were also reported, such as e.g., (HNEt$_3$)$^+$(Co^{II}Co$^{III}_3$L$_6$)$^-$, D/hc = –115 cm^{-1}. However, symmetry of this structure is D$_3$ [86].

8. Summary

Magnetostructural D-correlations, i.e., dependence of the axial zero-field splitting parameter *D* *vs* the structural anisotropy parameter D_{str} originate in the electronic structure of the central atom. They are tuned by the ligand diversity and structural variability of the individual metal complexes. Intuitive linear relationships (as in hexacoordinate Ni(II) systems) not always are supported by deep theoretical analysis which can rationalize various types of non-linear dependences. This is the case of the hexa-, penta- and tetracoordinate Co(II) complexes. Magnetostructural D-correlations represent an effective tool for the design of magnetically anisotropic molecules. Only from the knowledge of structural characteristics of the complexes can the magnitude and sign of the axial zero-field splitting parameter *D* be predicted, which enables the creation of relevant prediction models using contemporary machine learning methods [87].

Supplementary Materials: The following supporting information can be downloaded at: www.mdpi.com/xxx/s1, Figure S1: FA biplot after varimax rotation for hexacoordinate Ni(II) complexes; Figure S2: PCA biplot for hexacoordinate Co(II) complexes; Table S1: title; Table S1: Review of the matrix elements between the atomic-term kets; Table S2: Energy level diagrams for selected d^n systems; Table S3: Hexacoordinate Ni(II) complexes-structural and magnetic parameters, statistics; Table S4: Hexcoordinate Co(II) complexes-structural and magnetic parameters, statistics; Table S5: Tetracoordinate Co(II) complexes-structural and magnetic parameters, statistics; Table S6: Pentacoordinate Co(II) complexes-structural and magnetic parameters, statistics; Data selections for multivariate methods.

Author Contributions: Conceptualization, J.T. and R.B.; methodology, J.T. and R.B.; validation, J.T., R.B. and C.R.; formal analysis, J.T., R.B. and C.R.; investigation, J.T., R.B. and C.R.; data curation, J.T., R.B. and C.R.; writing—original draft preparation, J.T., R.B. and C.R.; writing—review and editing, J.T., R.B. and C.R.; visualization, J.T., R.B. and C.R. All authors have read and agreed to the published version of the manuscript.

Acknowledgments: Slovak grant agencies (APVV-19-0087 and VEGA 1/0086/21) are acknowledged for the financial support.

Conflicts of Interest: The authors declare no conflict of interest.

References

1. Lis, T. Preparation, structure, and magnetic properties of a dodecanuclear mixed-valence manganese carboxylate. *Acta Crystallogr.* **1980**, *B36*, 2042-2046.
2. Caneschi, A.; Gatteschi, D.; Sessoli, R.; Barra, A.L.; Brunel, L.C.; Guillot, L.C. Alternating current susceptibility, high field magnetization, and millimeter band EPR evidence for a ground S = 10 state in [Mn12O12(Ch3COO)16(H2O)4].2CH3COOH.4H2O. *J. Am. Chem. Soc.* **1991**, *133*, 5873-5874.
3. Aubin, S.M.J.; Wemple, M.W.; Adams, D.M.; Tsai, H.L.; Christou, G.; Hendrickson, D.N. Distorted MnIVMnIII3 Cubane Complexes as Single-Molecule Magnets. *J. Am. Chem. Soc.* **1996**, *118*, 7746-7754.
4. Gatteschi, D.; Sessoli, R.; Villain, J. *Molecular Nanomagnets*; Oxford University Press: 2006.
5. Mydosh, J.A. *Spin Glasses: An Experimental Introduction*; Taylor and Francis: London, 1995.
6. Winpenny, R. (Ed.). Single-Molecule Magnets and Related Phenomena. In *Structure and Bonding*; Springer: 2006; Volume 122.
7. Boča, R.; Rajnák, C. Unexpected behavior of single ion magnets. *Coord. Chem. Rev.* **2021**, *430*, 213657.
8. Rajnák, C.; Boča, R. Reciprocating thermal behavior in the family of single ion magnets. *Coord. Chem. Rev.* **2021**, *436*, 213808.
9. Rajnák, C.; Titiš, J.; Boča, R. Reciprocating Thermal Behavior in Multichannel Relaxation of Cobalt(ii) Based Single Ion Magnets. *Magnetochemistry* **2021**, *7*, 76.
10. Atzori, M.; Tesi, L.; Morra, E.; Chiesa, M.; Sorace, L.; Sessoli, R. Room-Temperature Quantum Coherence and Rabi Oscillations in Vanadyl Phthalocyanine: Toward Multifunctional Molecular Spin Qubits, *J. Am. Chem. Soc.* **2016**, *138*, 2154–2157.
11. Ding, M.; Cutsail, G.E.I.; Aravena, D.; Amoza, M.; Rouzières, M.; Dechambenoit, P.; Losovyj, Y.; Pink, M.; Ruiz, E.; Clérac, R. A low spin manganese(iv) nitride single molecule magnet. *Chem. Sci.* **2016**, *7*, 6132–6140.
12. Bhowmick, I.; Shaffer, D.W.; Yang, J.Y.; Shores, M.P. Single molecule magnet behaviour in a square planar S = 1/2 Co(ii) complex and spin-state assignment of multiple relaxation modes. *Chem. Commun.* **2020**, *56*, 6711–6714.
13. Chen, L.; Song, J.; Zhao, W.; Yi, G.; Zhou, Z.; Yuan, A.; Song, Y.; Wang, Z.; Ouyang, Z.W. A mononuclear five-coordinate Co(ii) single molecule magnet with a spin crossover between the S = 1/2 and 3/2 states. *Dalton Trans.* **2018**, *47*, 16596–16602.
14. Boča, R.; Mingos, D.M.P. (Eds.). *Theoretical Foundations of Molecular Magnetism*; Elsevier: Amsterdam, 1999.
15. Griffith, J.S. *The Theory of Transition Metal Ions*; Cambridge University Press: 1964.

16. Figgis, B.N. *Introduction to Ligand Fields*; Wiley: New York, 1966.
17. König, E.; Kremer, S. *Magnetism Diagrams for Transition Metal Ions*; Plenum Press: New York, 1979.
18. Boča, R. *Magnetic Functions Beyond the Spin-Hamiltonian*; Springer: 2006; Volume 117.
19. Boča, R. *A Handbook of Magnetochemical Formulae*; Elsevier: Amsterdam, 2012.
20. Crawford, V.H.; Richardson, H.W.; Wasson, J.R.; Hodgson, D.J.; Hatfield, W.E. Relation between the singlet-triplet splitting and the copper-oxygen-copper bridge angle in hydroxo-bridged copper dimers. *Inorg. Chem.* **1976**, 15, 2107–2110.
21. Hatfield, W.E.; Willett, R.D.; Gatteschi, D.; Kahn, O. *Magneto-Structural Correlations in Exchange Coupled Systems*; NATO ASI Series Reidel: Dordrecht, 1985; p. 555.
22. Thompson, L.K.; Mandal, S.K.; Tandon, S.S.; Bridson, J.N.; Park, M.K. Magnetostructural Correlations in Bis(μ2-phenoxide)-bridged Macrocyclic Dinuclear Copper(ii) Complexes. Influence of Electron-withdrawing Substituents on Exchange Coupling, *Inorg. Chem.* **1996**, 35, 3117–3125.
23. Glerup, J.; Hodgson, D.J.; Pedersen, E. A Novel Correlation Between Magnetism and Structural Parameters in Superexchange Coupled Chromium(iii) Dimers. *Acta. Chem. Scand.* **1983**, 37a, 161–164.
24. Hodgson, D.J.; Willet, R.D.; Gatteschi, D.; Kahn, O. *Magneto-Structural Correlations in Exchange Coupled Systems*, NATO ASI Series Reidel: Dordrecht, 1985; p. 501.
25. Law, N.A.; Kampf, J.W.; Pecoraro, V.L. A magneto-structural correlation between the Heisenberg constant, J, and the Mn-O-Mn angle in [MnIV(μ-O)]2 dimers. *Inorg. Chim. Acta* **2000**, *297*, 252–264.
26. Gorun, S.M.; Lippard, S.J. Magnetostructural Correlations in Magnetically Coupled (.mu.-oxo)diiron(iii) Complexes. *Inorg. Chem.* **1991**, *30*, 1625–1630.
27. Vranovičová, B.; Boča, R. Magnetostructural J-Correlations in Fe(III) Complexes-A Revison. *Nova Biotechnol. Chim.* **2013**, *12*, 70–74.
28. Tokárová-Puterová, Z.; Mrázová, V.; Kožíšek, J.; Valentová, J.; Vranovičová, B.; Boča, R. Magnetostructural correlation in tetracopper(II) cubanes. *Polyhedron* **2014**, *70*, 52–58.
29. Makohusová, M.; Mrázová, V.; Haase, W.; Boča, R. Magnetostructural J-correlations in complexes with tetrahedro-{Cu4} core. *Polyhedron* **2014**, *81*, 572–582.
30. Baran, P.; Boča, M.; Boča, R.; Krutošíková, A.; Miklovič, J.; Pelikán, J.; Titiš, J. Structural characterization, spectral and magnetic properties of isothiocyanate nickel(II) complexes with furopyridine derivatives. *Polyhedron* **2005**, *24*, 1510–1516.
31. Mašlejová, A.; Ivaniková, R.; Svoboda, I.; Papánková, B.; Dlháň, L.; Mikloš, D.; Fuess, H.; Boča, R. Structural characterization and magnetic properties of hexakis(imidazole)nickel(II) bis(formate), bis(chloroacetate), bis(2-chloropropionate) and hexakis(1-methyl-imidazole)nickel(II) chloride dihydrate. *Polyhedron* **2006**, *25*, 1823–1830.
32. Ivaniková, R.; Boča, R.; Dlháň, L.; Fuess, H.; Mašlejová, A.; Mrázová, V.; Svoboda, I.; Titiš, J. Heteroleptic nickel(II) complexes formed from N-donor bases, carboxylic acids and water: Magnetostructural correlations. *Polyhedron* **2006**, *25*, 3261–3268.
33. Titiš, J.; Boča, R.; Dlháň, Ľ.; Ďurčeková, T.; Fuess, H.; Ivaniková, R.; Mrázová, V.; Papánková, B.; Svoboda, I. Magnetostructural correlations in heteroleptic nickel(II) complexes. *Polyhedron* **2007**, *26*, 1523–1530.
34. Boča, R.; Titiš, J. *Coordination Chemistry Research Progress*; Nova Science Publishers: New York, 2008; p. 247.
35. Titiš, J.; Boča, R. Magnetostructural D Correlation in Nickel(II) Complexes: Reinvestigation of the Zero-Field Splitting. *Inorg. Chem.* **2010**, *49*, 3971–3973.
36. Packová, A.; Miklovič, J.; Titiš, J.; Koman, M.; Boča, R. Positive Zero-field Splitting in a Hexacoordinate Nickel(ii) Complex. *Inorg. Chem. Commun.* **2013**, *32*, 9–11.
37. Miklovič, J.; Packová, A.; Segľa, P.; Titiš, J.; Koman, M.; Moncoľ, J.; Boča, R.; Jorík, V.; Krekuska, H.; Valigura, D. Synthesis, Crystal Structures, Spectral and Magnetic Properties of Nickel(ii) Pyridinecarboxylates with N-heterocyclic Ligands. *Inorg. Chim. Acta* **2015**, *429*, 73–80.
38. Papánková, B.; Boča, R.; Dlháň, Ľ.; Nemec, I.; Titiš, J.; Svoboda, I.; Fuess, H. Magneto-structural relationships for a mononuclear Co(II) complex with large zero-field splitting. *Inorg. Chim. Acta* **2010**, *363*, 147–156.
39. Hudák, J.; Boča, R.; Dlháň, Ľ.; Kožíšek, J.; Moncoľ, J. Structure and Magnetism of Mono-, Di-, and Trinuclear Benzoato Cobalt(ii) Complexes. *Polyhedron* **2011**, *30*, 1367–1373.
40. Rajnák, C.; Titiš, J.; Boča, R.; Moncol', J.; Padělková, Z. Self-assembled cobalt(II) Schiff base complex: synthesis, structure, and magnetic properties. *Monatsh. Chem.* **2011**, *142*, 789–795.
41. Miklovič, J.; Segľa, P.; Mikloš, D.; Titiš, J.; Herchel, R.; Melník, M. Copper(ii) and Cobalt(ii) Hydroxypyridinecarboxylates: Synthesis, Crystal Structures, Spectral and Magnetic Properties. *Chem. Pap.* **2008**, *62*, 464–471.
42. Segľa, P.; Miklovič, J.; Mikloš, D.; Titiš, J.; Herchel, R.; Moncoľ, J.; Kaliňáková, B.; Hudecová, D.; Mrázová, V.; Lis, T. Crystal structure, spectroscopic and magnetic properties, and antimicrobial activities of cobalt(II) 2-methylthionicotinate complexes with N-heterocyclic ligands. *Trans. Met. Chem.* **2008**, *33*, 967–974.

43. Titiš, J.; Hudák, J.; Kožíšek, J.; Krutošíková, A.; Moncoľ, J.; Tarabová, D.; Boča, R. Structural, Spectral and Magnetic Properties of Carboxylato Cobalt(ii) Complexes with Heterocyclic N-donor Ligands: Reconstruction of Magnetic Parameters from Electronic Spectra. *Inorg. Chim. Acta* **2012**, *388*, 106–113.
44. Šebová, M.; Boča, R.; Dlháň, Ľ.; Nemec, I.; Papánková, B.; Pavlik, J.; Fuess, H. Direct determination of zero-field splitting in Co(II) complexes by FAR infrared spectroscopy. *Inorg. Chim. Acta* **2012**, *383*, 143–151.
45. Titiš, J.; Boča, R. Magnetostructural D Correlations in Hexacoordinated Cobalt(ii) Complexes. *Inorg. Chem.* **2011**, *50*, 11838–11845.
46. Idešicová, M.; Boča, R. Magnetism, IR and Raman spectra of a tetracoordinate and hexacoordinate Co(II) complexes derived from aminopyrimidine. *Inorg. Chim. Acta* **2013**, *408*, 162–171.
47. Váhovská, L.; Potočňák, I.; Vitushkina, S.; Dušek, M.; Titiš, J.; Boča, R. Low-dimensional compounds containing cyanido groups. XXVI. Crystal structure, spectroscopic and magnetic properties of Co(II) complexes with non-linear pseudohalide ligands. *Polyhedron* **2014**, *81*, 396–408.
48. Herchel, R.; Váhovská, L.; Potočňák, I.; Trávníček, Z. Slow Magnetic Relaxation in Octahedral Cobalt(II) Field-Induced Single-Ion Magnet with Positive Axial and Large Rhombic Anisotropy. *Inorg. Chem.* **2014**, *53*, 5896–5898.
49. van Stapele, R.P.; Beljers, H.G.; Bongers, P.F.; Zijlstra, H. Ground State of Divalent Co Ions in Cs3CoCl5 and Cs3CoBr5. *J. Chem. Phys.* **1966**, *44*, 3719–3725.
50. Krzystek, J.; Zvyagin, S.A.; Ozarowski, A.; Fiedler, A.T.; Brunold, T.C.; Telser, J. Definitive Spectroscopic Determination of Zero-Field Splitting in High-Spin Cobalt(II). *J. Am. Chem. Soc.* **2004**, *126*, 2148–2155.
51. Idešicová, M.; Titiš, J.; Krzystek, J.; Boča, R. Zero-Field Splitting in Pseudotetrahedral Co(II) Complexes: A Magnetic, High-Frequency and -Field EPR, and Computational Study. *Inorg. Chem.* **2013**, *52*, 9409–9417.
52. Šebová, M.; Jorík, V.; Kožíšek, J.; Moncoľ, J.; Boča, R. Structure and Magnetism of Co(ii) Complexes with Bidentate Heterocyclic Ligand Hsalbim Derived from Benzimidazole. *Polyhedron* **2011**, *30*, 1163–1170.
53. Idešicová, M.; Dlháň, Ľ.; Moncoľ, J.; Titiš, J.; Boča, R. Zero-field Splitting in Tetracoordinate Co(ii) Complexes. *Polyhedron* **2012**, *36*, 79–84.
54. Titiš, J.; Miklovič, J.; Boča, R. Magnetostructural study of tetracoordinate cobalt(II) complexes. *Inorg. Chem. Commun.* **2013**, *35*, 72–75.
55. Rajnák, C.; Titiš, J.; Šalitroš, I.; Boča, R.; Fuhr, O.; Ruben, M. Zero-field splitting in pentacoordinate Co(II) complexes. *Polyhedron* **2013**, *65*, 122–128.
56. Rajnák, C. Cyril and Methodius. Ph.D. Thesis, University of SS, Trnava, 2014.
57. Rajnák, C.; Titiš, J.; Miklovič, J.; Kostakis, G.E.; Fuhr, O.; Ruben, M.; Boča, R. Five Mononuclear Pentacoordinate Co(ii) Complexes with Field-induced Slow Magnetic Relaxation. *Polyhedron* **2017**, *126*, 174–183.
58. Rajnák, C.; Titiš, J.; Fuhr, O.; Ruben, M.; Boča, R. Single-Molecule Magnetism in a Pentacoordinate Cobalt(II) Complex Supported by an Antenna Ligand. *Inorg. Chem.* **2014**, *53*, 8200–8202.
59. Habib, F.; Luca, O.R.; Vieru, V.; Shiddiq, M.; Korobkov, I.; Gorelsky, S.I.; Takase, M.K.; Chibotaru, L.F.; Hill, S.; Crabtree, R.H.; et al. Influence of the Ligand Field on Slow Magnetization Relaxation versus Spin Crossover in Mononuclear Cobalt Complexes. *Angew. Chem. Int. Ed.* **2013**, *52*, 11290–11293.
60. Ishikawa, R.; Miyamoto, R.; Nojiri, H.; Breedlove, B.K.; Yamashita, M. Slow Relaxation of the Magnetization of an MnIII Single Ion. *Inorg. Chem.* **2013**, *52*, 8300–8302.
61. Grigoropoulous, A.; Pissas, M.; Rapatolis, P.; Psycharis, V.; Kyritsis, P.; Sanakis, Y. Spin-relaxation Properties of a High-spin Mononuclear Mniiio6-containing Complex. Spin-Relaxation Properties of a High-Spin Mononuclear MnIIIO6-Containing Complex. *Inorg. Chem.* **2013**, *52*, 12869–12871.
62. Vallejo, J.; Pascual-Alvarez, A.; Cano, J.; Castro, I.; Julve, M.; Lloret, F.; Krzystek, J.; De Munno, G.; Armentano, D.; Wernsdorfer, W.; Ruiz-Garcia, R.; Pardo, E. Field-induced Hysteresis and Quantum Tunneling of the Magnetization in a Mononuclear Manganese(iii) Complex. Field-Induced Hysteresis and Quantum Tunneling of the Magnetization in a Mononuclear Manganese(III) Complex. *Angew. Chem. Int. Ed.* **2013**, *125*, 14325–14329.
63. Mossin, S.; Tran, B.L.; Adhikari, D.; Pink, M.; Heinemann, F.W.; Sutter, J.; Szilagyi, R.K.; Meyer, K.; Mindiola, D.J. A Mononuclear Fe(III) Single Molecule Magnet with a 3/2↔5/2 Spin Crossover. *J. Am. Chem. Soc.* **2012**, *134*, 13651–13661.
64. Harman, W.H.; Harris, T.D.; Freedman, D.E.; Fong, H.; Chang, A.; Rinehart, J.D.; Ozarowski, A.; Sougrati, M.T.; Grandjean, F.; Long, G.J.; et al. Slow Magnetic Relaxation in a Family of Trigonal Pyramidal Iron(ii) Pyrrolide Complexes. Slow Magnetic Relaxation in a Family of Trigonal Pyramidal Iron(II) Pyrrolide Complexes. *J. Am. Chem. Soc.* **2010**, *132*, 18115–18126.
65. Freedman, D.E.; Harman, W.H.; Harris, T.D.; Long, G.J.; Chang, C.J.; Long, J.R. Slow Magnetic Relaxation in a High-spin Iron(ii) Complex. *J. Am. Chem. Soc.* **2010**, *132*, 1224–1225.
66. Weismann, D.; Sun, Y.; Lan, Y.; Wolmershauser, G.; Powell, A.K.; Sitzmann, H. High-Spin Cyclopentadienyl Complexes: A Single-Molecule Magnet Based on the Aryl-Iron(II) Cyclopentadienyl Type. *Chem. Eur. J.* **2011**, *17*, 4700–4704.

67. Lin, P.-H.; Smythe, N.C.; Gorelsky, S.J.; Maguire, S.; Henson, N.J.; Korobkov, I.; Scott, B.L.; Gordon, J.C.; Baker, R.T.; Murugesu, M. Importance of Out-of-state Spin–orbit Coupling for Slow Magnetic Relaxation in Mononuclear Feii Complexes. *J. Am. Chem. Soc.* **2011**, *133*, 15806–15809.
68. Zadrozny, J.M.; Xiao, D.J.; Atanasov, M.; Long, G.J.; Grandjean, F.; Neese, F.; Long, J.R. Magnetic Blocking in a Linear Iron(i) Complex. *Nat. Chem.* **2013**, *5*, 577–581.
69. Eichhofer, A.; Lan, Y.; Mereacre, V.; Bodenstein, T.; Weigend, F. Slow Magnetic Relaxation in Trigonal-planar Mononuclear Fe(ii) and Co(ii) Bis(trimethylsilyl)amido Complexes—A Comparative Study. *Inorg. Chem.* **2014**, *55*, 1962–1974.
70. Zadrozny, J.M.; Long, J.R. Slow Magnetic Relaxation at Zero Field in the Tetrahedral Complex [Co(SPh)4]2–. *J. Am. Chem. Soc.* **2011**, *133*, 20732–20734.
71. Zadrozny, J.M.; Liu, J.; Piro, N.A.; Chang, C.J.; Hill, S.; Long, J.R. Slow Magnetic Relaxation in a Pseudotetrahedral Cobalt(ii) Complex with Easy-plane Anisotropy. *Chem. Commun.* **2012**, *48*, 3927–3929.
72. Yang, F.; Zhou, Q.; Zhang, Y.; Zeng, G.; Li, G.; Shi, Z.; Wang, B.; Feng, S. Inspiration from Old Molecules: Field-induced Slow Magnetic Relaxation in Three Air-stable Tetrahedral Cobalt(ii) Compounds. *Chem. Commun.* **2013**, *49*, 5289–5291.
73. Boča, R.; Miklovič, J.; Titiš, J. Simple Mononuclear Cobalt(ii) Complex: A Single-molecule Magnet Showing Two Slow Relaxation Processes. *Inorg. Chem.* **2014**, *53*, 2367–2369.
74. Jurca, T.; Farghal, A.; Lin, P.-H.; Korobkov, I.; Murugesu, M.; Richeson, D.S. Single-Molecule Magnet Behavior with a Single Metal Center Enhanced through Peripheral Ligand Modifications. *J. Am. Chem. Soc.* **2011**, *133*, 15814–15817.
75. Vallejo, J.; Castro, I.; Ruiz-Garcia, J.; Cano, J.; Julve, M.; Lloret, F.; De Munno, G.; Wernsdorfer, W.; Pardo, E. Field-induced Slow Magnetic Relaxation in a Six-coordinate Mononuclear Cobalt(ii) Complex with a Positive Anisotropy. *J. Am. Chem. Soc.* **2012**, *134*, 15704–15707.
76. Colacio, E.; Ruiz, K.; Ruiz, E.; Cremades, E.; Krzystek, J.; Carretta, S.; Cano, J.; Guidi, T.; Wernsdorfer, W.; Brechin, E.K. Slow Magnetic Relaxation in a Coii–yiii Single-ion Magnet with Positive Axial Zero-field Splitting. *Angew. Chem. Int. Ed.* **2013**, *125*, 9300–9304.
77. Zhu, Y.-Y.; Cui, C.; Zhang, Y.-Q.; Jia, J.-H.; Guo, X.; Gao, C.; Qian, K.; Jiang, S.-D.; Wang, B.-W.; Wang, Z.-M. Zero-field slow magnetic relaxation from single Co(ii) ion: A transition metal single-molecule magnet with high anisotropy barrier. *Chem. Sci.* **2013**, *4*, 1802–1806.
78. Makinen, M.V.; Kuo, L.C.; Yim, M.B.; Wells, G.B.; Fukuyama, J.M.; Kim, J.E. Ground Term Splitting of High-spin Cobalt(2+) Ion as a Probe of Coordination Structure. 1. Dependence of the Splitting on Coordination Geometry. *J. Am. Chem. Soc.* **1985**, *107*, 5245–5255.
79. Neese, F.; Solomon, R.I. Calculation of Zero-Field Splittings, g-Values, and the Relativistic Nephelauxetic Effect in Transition Metal Complexes. Application to High-Spin Ferric Complexes. *Inorg. Chem.* **1998**, *37*, 6568–6582.
80. Maganas, D.; Krzystek, J.; Ferentinos, E.; Whyte, A.M.; Robertson, N.; Psycharis, V.; Terzis, A.; Neese, F.; Kyritsis, P. Investigating Magnetostructural Correlations in the Pseudooctahedral Trans-[niii{(opph2)(epph2)n}2(sol)2] Complexes (E = S, Se; Sol = DMF, THF) by Magnetometry, HFEPR, and Ab Initio Quantum Chemistry. *Inorg. Chem.* **2012**, *51*, 7218–7231.
81. Duboc, C.; Ganyushin, D.; Sivalingam, K.; Collomb, M.-N.; Neese, F. Systematic Theoretical Study of the Zero-field Splitting in Coordination Complexes of Mn(iii). Density Functional Theory Versus Multireference Wave Function Approaches. *J. Phys. Chem. A* **2010**, *114*, 10750–10758.
82. Carlin, R.L. *Magnetochemistry*; Springer: Berlin, 1986.
83. Boča, R.; Dlháň, Ľ.; Haase, W.; Herchel, R.; Mašlejová, A.; Papánková, B. Limiting Negative Zero-field Splitting in Tetrakis(imidazole)bis(acetato) Nickel(ii) Complex. *Chem. Phys. Lett.* **2003**, *373*, 402–410.
84. Boča, R. Zero-field splitting in metal complexes. *Coord. Chem. Rev.* **2004**, *248*, 757–815.
85. Neese, F. Importance of Direct Spin−spin Coupling and Spin-flip Excitations for the Zero-field Splittings of Transition Metal Complexes: A Case Study. *J. Am. Chem. Soc.* **2006**, *128*, 10213–10222.
86. Zhu, Y.Y.; Cui, C.; Zhang, Y.Q.; Jia, J.H.; Guo, X.; Gao, C.; Qian, K.; Jiang, S.D.; Wang, B.W.; Wang, Z.M. Zero-field slow magnetic relaxation from single Co(ii) ion: a transition metal single-molecule magnet with high anisotropy barrier. *Chem. Sci.* **2013**, *4*, 1802–1806.
87. Kulik, H.J. Making machine learning a useful tool in the accelerated discovery of transition metal complexes. *WIREs Comput. Mol. Sci.* **2019**, e1439.